metals

MDPI

Article

Dry Sliding Tribological Properties of a Hard Anodized AA6082 Aluminum Alloy

Eleonora Santecchia [1,*], Marcello Cabibbo [1], Abdel Magid Salem Hamouda [2], Farayi Musharavati [2], Anton Popelka [3] and Stefano Spigarelli [1]

1 Dipartimento di Ingegneria Industriale e Scienze Matematiche (DIISM), Università Politecnica delle Marche, Via Brecce Bianche 12, 60131 Ancona, Italy; m.cabibbo@univpm.it (M.C.); s.spigarelli@univpm.it (S.S.)
2 Mechanical and Industrial Engineering Department, College of Engineering, Qatar University, Doha 2713, Qatar; hamouda@qu.edu.qa (A.M.S.H.); farayi@qu.edu.qa (F.M.)
3 Center for Advanced Materials, Qatar University, Doha 2713, Qatar; anton.popelka@qu.edu.qa
* Correspondence: e.santecchia@univpm.it; Tel.: +39-0712-204-731

Received: 30 December 2019; Accepted: 28 January 2020; Published: 1 February 2020

Abstract: The applications of aluminum and its alloys are still limited by low hardness and low wear resistance properties. Surface modifications, such anodizing and plasma electrolytic oxidation, represent a feasible way to overcome these drawbacks. In this study, discs of AA6082 were subjected to the so-called G.H.A. hard anodizing process leading to an anodized layer having a honeycomb-like structure. Samples having alumina layer thicknesses of 10, 50 and 100 µm were subjected to unidirectional dry sliding wear tests, using bearing steel and silicon nitride as counterbody materials. Surface and structure characterization of the samples were performed before and after the tribological tests, using a wide range of techniques; atomic force microscopy and scanning electron microscopy techniques were used before the wear tests. The wear scars were characterized by scanning electron microscopy, energy dispersive spectroscopy and Fourier transform infrared spectroscopy techniques. Results show that the different thickness of the anodized layer does not affect the pores dimensions but has an influence on the micrometric domains in which the pores are divided. These features coupled with the wear test conditions, show to have a strong influence on the wear behavior. The thinnest sample showed also the best performance against the ceramic counterbody.

Keywords: hard anodizing; AA6082; dry sliding; friction

1. Introduction

Aluminum and its alloys are widely used in a variety of industrial fields, owing to their low density, good thermal and electrical conductivity and high strength. However, the practical applications of these materials result in being still limited by major drawbacks like low hardness and poor wear resistance. A feasible way to overcome these issues is to implement processes that modify surfaces, such as anodizing, thermal spraying and plasma electrolytic oxidation.

The aluminum alloys 6xxx series are of particular interest for both the aerospace and automotive industries, owing to the combination of intrinsic properties such as medium strength, formability, weldability and corrosion resistance, coupled with the low cost [1,2].

Among all the alloys belonging to the 6xxx series, the precipitation-hardenable medium-strength AA6082 is characterized by an excellent corrosion resistance and shows also the highest strength in the 6xxx series [3,4]. These peculiar properties coupled with the high strength-to-weight ratio and specific stiffness, are the reasons behind the extensive application of this Al–Mg–Si alloy in automotive, aerospace and shipbuilding industries [5–8].

The spontaneous oxidation taking place on the surface of aluminum is the fundamental basic of the anodizing process, involving also a proper temperature level, an electrolytic solution, and the electrical current [9,10]. During the process, the aluminum piece is placed inside the electrolytic bath and is connected to the positive side (cathode) of a DC power supply, while the anode (negative side) is an inert metal. When the current flows into the circuit, aluminum reacts with the electrolytic bath, building up an Al_2O_3 oxide layer [11,12].

The mechanical and tribological properties of the oxide layer obtained by the anodizing process are strongly influenced by the Al_2O_3 porosity and thickness [13–15]. These, in turn, strongly depend on the operating conditions of the anodizing process, such as the cell voltage and the electrolyte composition [16–21].

The porosity of the anodic oxide layers was found to be beneficial for tribological applications, being used as a reservoir for lubricants to form self-lubricating structures, enhancing the friction and wear performances [22–24]. Extensive studies on the wear resistance of filled-in anodic aluminum oxide (AAO), as well as filled-up with solid or liquid lubricants, have been carried out [15,25–31], but not many papers deal with the wear properties of anodized aluminum alloys under a dry (non-lubricated) environment [14,32–37]. It is even harder to find a paper that investigated the dry sliding performance of hard anodized aluminum under medium normal loads (between 1 and 10 N).

Vengatesh et al. [38] developed procedures to grow anodic aluminum oxide layers with self-lubricating properties, which were successfully tested under 10 N normal load against stainless steel (301), obtaining the coefficient of friction values always lower than 0.2. Tsyntsaru et al. [37] tested the wear and friction behavior of anodic aluminum oxide (AAO) against corundum balls under normal loads ranging from 40 to 1000 mN, with the resulting coefficient of friction values, which vary with the porosity of the anodized layer; the formation of debris layers on top of the anodized surface was also observed. The performance of 1050A and 5754H111 alloys anodized in different conditions were tested by Guezmil et al. [32] under a load of 1 N against 100Cr6 counterbodies, showing a complex wear mechanism affected by many factors including the initial morphology of the anodized layer.

Higher loads were tested by Dejun et al. [39] against ceramic counterbodies showing the dominance of abrasive wear. Furthermore, Lu et al. [40] studied the wear of AA2024 subjected to anodization with a novel acid bath mixture, using 100Cr6 steel as counterbody material under a normal load of 10 N; results show that the surface properties of the anodized layer have a strong influence on the wear and friction behavior of the tested samples. Recently, anodized eutectic Al–Si alloys were tested at higher loads (20 N) against nodular cast iron [41], while medium loads (5 N) and corundum balls were used by Benea et al. [42] to study the friction and wear performance of anodic films grown using different potential, showing wear rates always lower than 2×10^{-3} mm^3/Nm.

In the present study, discs of aluminum alloy 6082 were subjected to a particular hard anodizing process [43,44], and their wear performance was characterized through unidirectional dry sliding tests. The surface and microstructure of the samples was characterized coupling different techniques and correlated to the conditions at which the wear tests were performed.

2. Materials and Methods

Disc specimens having a diameter of 20 mm and a thickness of 5 mm made of aluminum alloy 6082 T6 were subjected to the hard anodizing treatment known as G.H.A.® [44]. The main feature of this method is represented by sealing the Al_2O_3 layer porosities with silver ions. Moreover, this particular anodizing process creates a compact hexahedral alumina layer organized in a honeycomb-like structure. According to the different anodized layer thickness, samples were divided in three groups: (i) 10 μm (GHA10), (ii) 50 μm (GHA50) and (iii) 100 μm (GHA100), as shown in Table 1.

Table 1. Description of the characterized samples.

Name	Al_2O_3 Thickness
GHA10	10 μm
GHA50	50 μm
GHA100	100 μm

Surface morphology was detected by means of atomic force microscopy (AFM), using an MFP-3D AFM device (Asylum Research, Goleta, CA, USA); for each sample, regions having a surface area of 1 μm × 1 μm were inspected.

Microhardness measurements were performed using an applied load of 200 gf using a REMET HX1000 machine (Remet, Bologna, Italy). Each data is the average of five individual measurements.

The friction coefficients were measured using unidirectional dry sliding pin-on-disk wear tests, performed by means of a tribometer (VTHT, Anton-Paar®, Buchs, Switzerland). Tribological experiment were conducted in ambient atmospheric conditions at a room temperature of about 20 ± 2 °C, and at a relative humidity of about 75%. In order to fully characterize the wear behavior of the anodized coatings, two different balls materials were chosen as counterbodies: (i) bearing steel 100Cr6 and (ii) ceramic (Si_3N_4). The diameter of the balls was 6 mm. The maximum surface roughness values of the metallic and ceramic balls were 0.032 μm and 0.014 μm, respectively. The main experimental parameters for the tribological tests were set as follows: (i) 5 N normal load, (ii) 6 mm track radius, (iii) total distance of 250 m, and (iv) a linear speed of 10 cm/s. To ensure the repeatability of the results, three tribotests have been performed for each condition. In order to have an exhaustive characterization of the dry sliding behavior of the samples, very hard (Si_3N_4, about 1600 HV) and softer (100Cr6, martensitic, about 700 HV) counterbody materials were used, while the remaining testing conditions were unchanged.

Wear tracks were characterized by field emission gun scanning electron microscopy (FEGSEM) using a FEI (FEI, Eindhoven, The Netherlands) Nova NanoSEM equipped with a Bruker Quantax (Bruker, Hamburg, Germany) energy dispersive spectroscopy (EDS) unit for elemental microanalysis.

The SEM micrographs were obtained collecting the secondary electrons signal and using 5 kV accelerating voltage.

Chemical analysis of the tracks was performed with the Fourier Transform Infrared Spectroscopy (FTIR) technique, using a Perkin Elmer Spectrum 400 spectrometer (Perkin Elmer, Waltham, MA, USA).

The images and profiles of the wear tracks from the 876.6 μm × 659.8 μm surface area were acquired by profilometry analysis using an optical surface metrology system Leica DCM8 (Leica Microsystems, Wetzlar, Germany) with an EPI 20X-L objective. The specific wear rate W was calculated using the normal load N, the sliding distance S and the wear volume V [45,46], which was calculated using the wear track depth and width information from the profiles examined at the optical profilometer.

3. Results

3.1. Microstructural Characterization

In order to characterize the surface morphology, the three GHA samples, namely the GHA10, GHA50 and GHA100 samples, were investigated by atomic force microscopy (AFM).

The 1 μm × 1 μm images reported in Figure 1 show remarkable differences among the surfaces of the samples. The surface of the GHA10 sample (Figure 1a) shows semi-parallel deep grooves that disappear when the thickness of the anodized layer was increased up to 50 μm. In fact, on the GHA50 surface (Figure 1b) only rounded dimples and bubble-like features were visible. When the thickness of the alumina layer was further increased up to 100 μm, the surface results to be a combination of the peculiarities shown by the first two samples; indeed, a quite smooth surface with small rounded features organized in shallow grooves was present (Figure 1c).

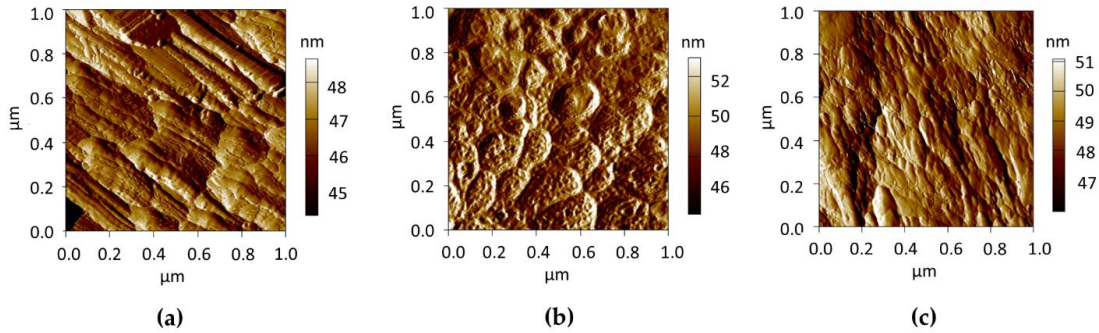

Figure 1. Atomic force microscopy (AFM) images of the samples surfaces: (**a**) GHA10, (**b**) GHA50 and (**c**) GHA100.

In order to deeply characterize the surface of the samples, the field emission gun scanning electron microscope was used. Figure 2 shows the micrographs obtained with the secondary electrons signal.

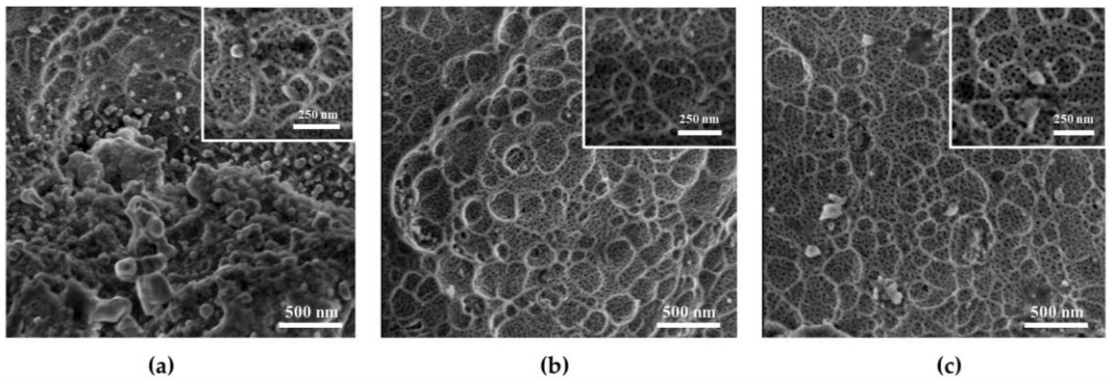

Figure 2. Field emission gun scanning electron microscopy (FEGSEM) inspection of the samples surfaces: (**a**) GHA10, (**b**) GHA50 and (**c**) GHA100. Insets show high magnification details.

In this particular case, the electronic beam was accelerated by a low voltage (i.e., not higher than 3 kV), with the purpose to limit the charge effects and keep the detailed level of the images as high as possible, avoiding the application of a conductive coating. The micrograph in Figure 2a shows that the GHA10 samples had peculiar superficial features not detectable on the other samples. The structure of the porous anodic aluminum oxide (AAO) was organized in domains having variable dimensions and a spherical shape. The insets show high magnification details, highlighting the presence of smaller domains (sub-domains) and the characteristic porosity of the anodized samples. In the inset of Figure 2a, a less ordered structure of the domains was visible, owing to the particular features of this sample. As can be seen from Figure 2, the porosity did not change remarkably in the three conditions. The mean pore diameter was calculated from the micrographs using stereological methods and the resulting value was 13 ± 2 nm for the GHA10 and GHA50 samples, and 14 ± 3 nm for the GHA100.

In order to highlight the adhesion of the anodized layer to the AA6082 substrate, FEGSEM images on the cross-sections of the samples before the tribotests were acquired and the results are shown in Figure 3.

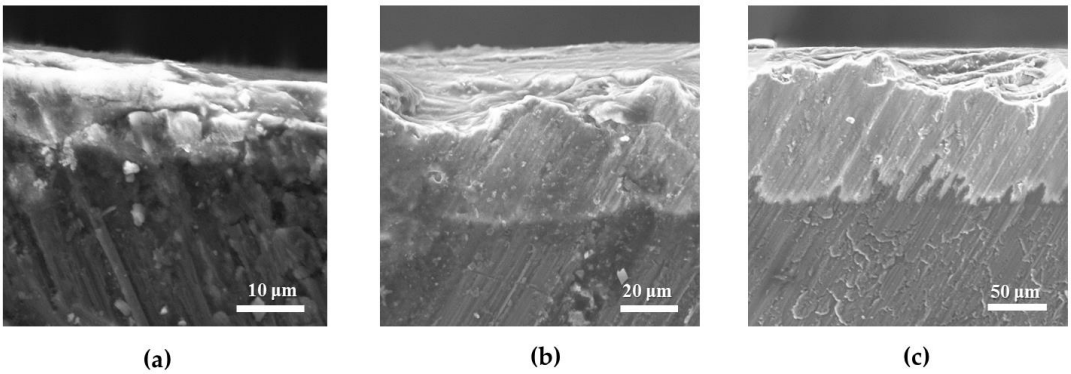

Figure 3. FEGSEM cross sections of the samples (from left to right: (**a**) GHA10, (**b**) GHA50 and (**c**) GHA100).

The micrographs in Figure 3 highlight the absence of cracks at the interface between the substrate and the anodized layer. It is worth to note that the scale bar is different in each of the three micrographs to better visualize the interface.

Microhardness of all the anodized samples was measured and the results are reported in Table 2.

Table 2. Microhardness values measured for all the anodized samples.

Sample	Microhardness (HV)
GHA10	310 ± 30
GHA50	260 ± 20
GHA100	350 ± 30

It is worth to note that the microhardness value of the GHA50 was the lowest, while considering the standard deviations highlighted in Table 2, the other two samples show similar values.

3.2. Wear Behavior

Unidirectional dry sliding wear tests were performed using bearing steel (100Cr6) and ceramic (Si_3N_4) balls as counterbodies. Figure 4 shows the evolution of the friction coefficient (COF or rather μ as shown in all the graphs) for the three samples sliding against the two counterbody materials, as a function of the sliding distance.

The friction coefficient evolutions reported in Figure 4 showed remarkable differences in the sliding behavior against the ceramic and metallic counterbodies. The black lines refer to the ceramic balls, while those in blue correspond to the metallic ones. The GHA/Si_3N_4 tribo-system showed a typical trend of the friction coefficient, with an initial strong increase (running-in period), followed by a steady-state wear regime, where the COF remained constant. The black curves did not show any remarkable variation along the 250 m of sliding distance and the highest value reached by the friction coefficient was 0.93 for all the tested samples. The GHA/100Cr6 tribo-system showed a running-in period as well at the beginning of the sliding movement, but the following steady-state regime was characterized by a higher instability of the friction coefficient value. This effect was particularly marked when the GHA10 samples slide against the steel counterbodies as reported in Figure 4a, being the running-in period the longest measured, with a duration of 60 m. It is worth to note that, although the evolution of the COF was quite different for the three samples during the tests against 100Cr6, the average COF values (Figure 4d) calculated from the steady state regime were quite similar.

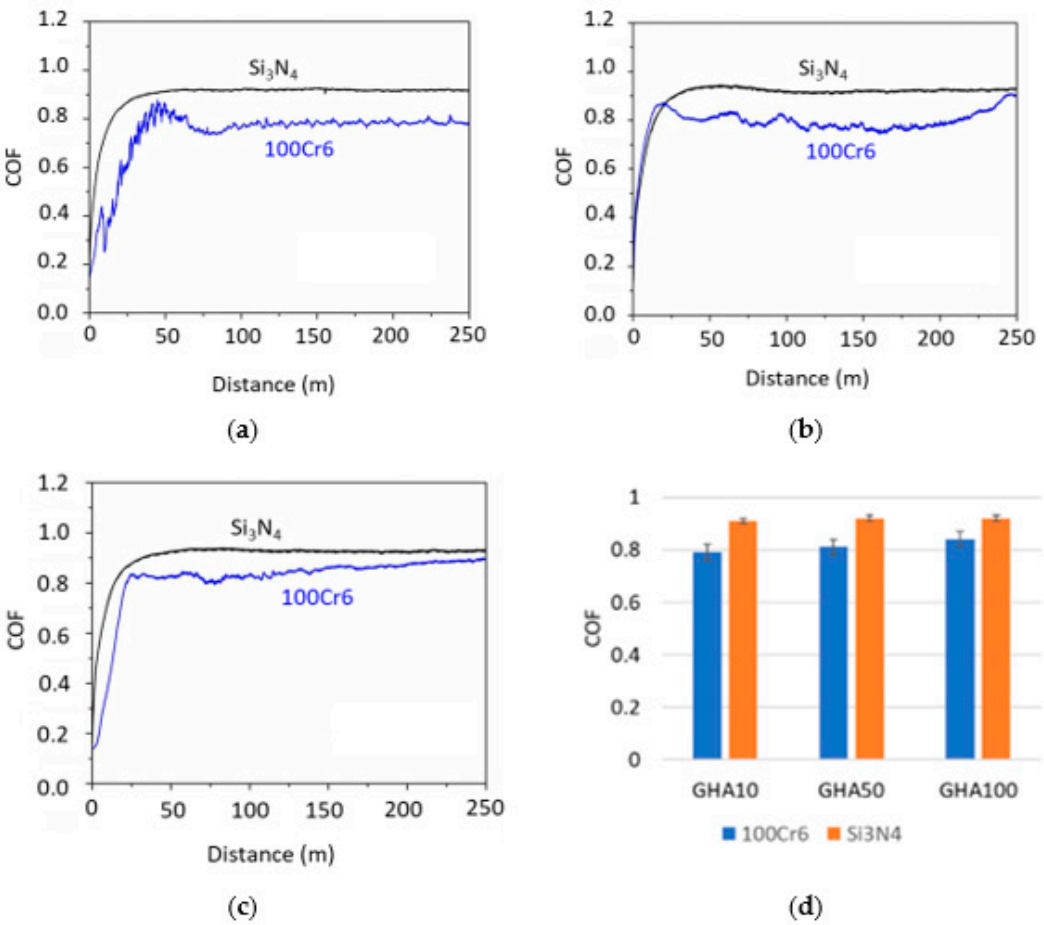

Figure 4. Friction coefficient evolution for (**a**) GHA10, (**b**) GHA50, (**c**) GHA10 and average friction coefficient (COF) values (**d**).

Figure 5 shows the FEGSEM micrographs of the wear tracks due to the dry sliding of the GHA samples against 100Cr6 balls. Upper row (Figure 5a–c) shows the overview of the wear tracks at low magnification, while the lower row (Figure 5d–f) shows a higher magnification of the scars' details.

The GHA50 (Figure 5b) and GHA100 (Figure 5c) scars were quite smooth and grooves parallel to the sliding direction were visible. The high magnification micrographs of these two samples (Figure 5e,f) highlighted the cracks formation inside the wear tracks, leading to the fragmentation of the wear surfaces in big flakes. The spotted flakes were smaller in the GHA100 sample (Figure 5f), with respect to those in Figure 5e. A peculiar behavior could be once again spotted for the GHA10 samples after sliding against the metallic counterbodies (Figure 5a,d). In this case, a large amount of debris was deposited over the wear track and on its borders, and the high magnification micrograph (Figure 5d) clearly showed the presence of a dense layer with a few deep cracks perpendicular to the sliding direction.

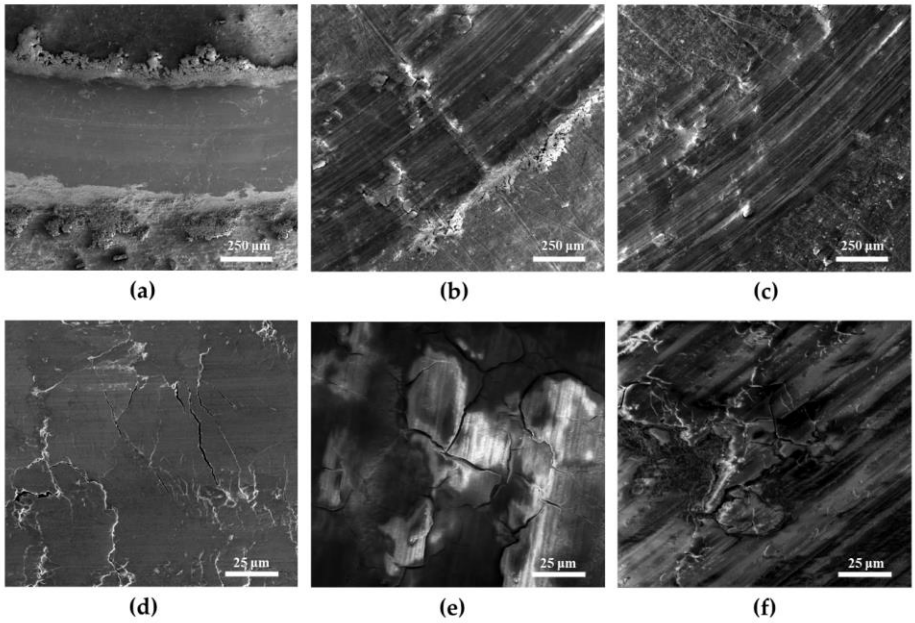

Figure 5. Wear tracks of the GHA/100Cr6 system. Low magnification of: (**a**) GHA10, (**b**) GHA50 and (**c**) GHA100. High magnification of the inner details: (**d**) GHA10, (**e**) GHA50 and (**f**) GHA100.

The wear profile tracks confirmed the peculiar results of the GHA10/100Cr6 tribocouple, evidenced by the FEGSEM inspections. The same peculiar layer covering the wear track shown in Figure 5a was visible also in Figure 6a and the profile scan highlighted that this was material deposited on the track (build-up of material instead of consumption). On the other hand, wear tracks of the GHA50 and GHA100 samples show the accumulations of wear debris at the edges of the wear tracks and a higher amount of material ripped off in the case of the GHA100/100Cr6 tribocouple (Figure 6c).

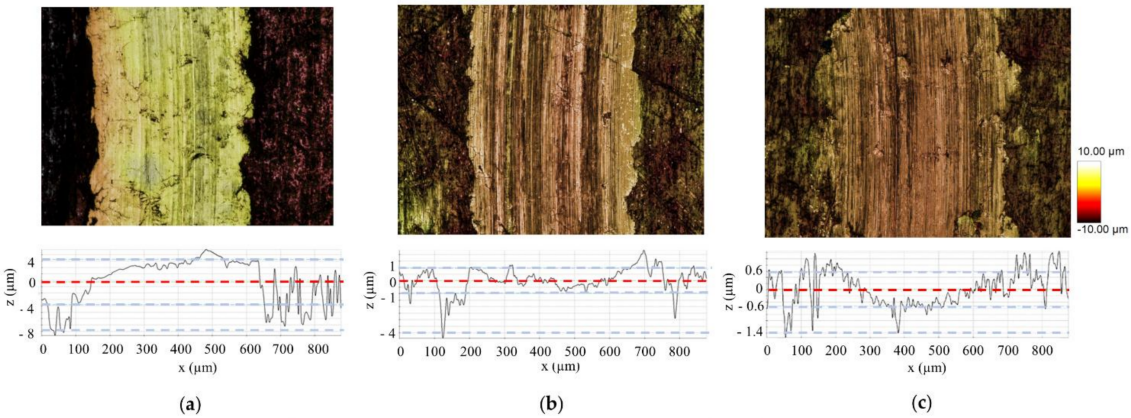

Figure 6. Optical profilometry of wear tracks for the GHA/100Cr6 system: (**a**) GHA10, (**b**) GHA50 and (**c**) GHA100.

The FEGSEM micrographs of the GHA/Si_3N_4 tribo-system were reported in Figure 7 (as in Figure 5) with the upper row (Figure 7a–c) showing the low magnification overview of the wear tracks, and the lower row (Figure 7d–f) highlighting the tracks details at high magnification.

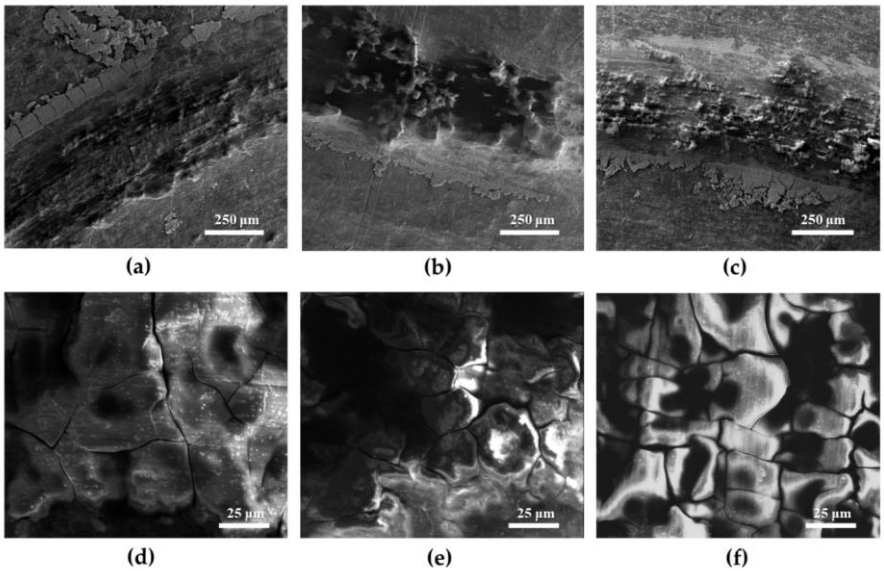

Figure 7. Wear tracks of the GHA/Si_3N_4 system. Low magnification of: (**a**) GHA10, (**b**) GHA50 and (**c**) GHA100. High magnification of the inner details: (**d**) GHA10, (**e**) GHA50 and (**f**) GHA100.

A high amount of wear debris was detected on the edges of the wear tracks, which in turn were characterized by grooves parallel to the sliding direction. High magnification micrographs (Figure 7d–f) highlighted the formation of flakes inside the wear track, and this effect was particularly remarkable as the anodized layer thickness rises. The formation of flakes is further enhanced for the GHA50 (Figure 7b,e) and GHA100 (Figure 7c–f) samples. The morphological details of the tracks suggested that fracture and delamination of the Al_2O_3 coating was the main wear mechanism.

Optical profilometry analysis of the wear tracks after dry sliding against silicon nitride are reported in Figure 8.

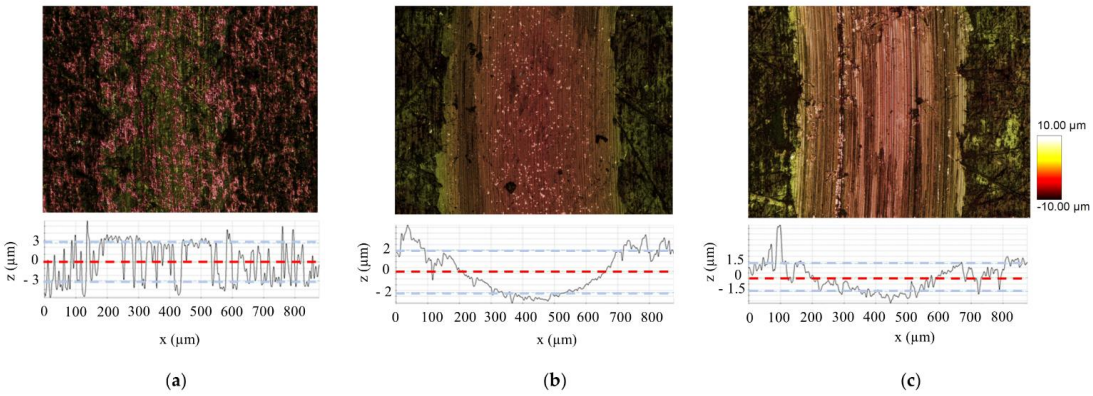

Figure 8. Optical profilometry of wear tracks of the GHA/Si_3N_4 system: (**a**) GHA10, (**b**) GHA50 and (**c**) GHA100.

It is worth to note that the wear of the GHA10 sample in this case was negligible (Figure 8a), while among the thicker anodized layers, the 50 µm (GHA50) showed to undergo a higher wear during the tests compared to the GHA100 (Figure 8b,c). As shown in Figure 8, spallation and consequent accumulation of a remarkable amount of debris at the edges of the wear tracks was detected for the GHA50 and GH100 samples, but not for the GHA10 one.

The profilometry results obtained for all the tested samples were used to calculate the wear volume [47], which was used to calculate the specific wear rate W (mm^3/Nm). The results of the wear rate calculations are reported in Figure 9.

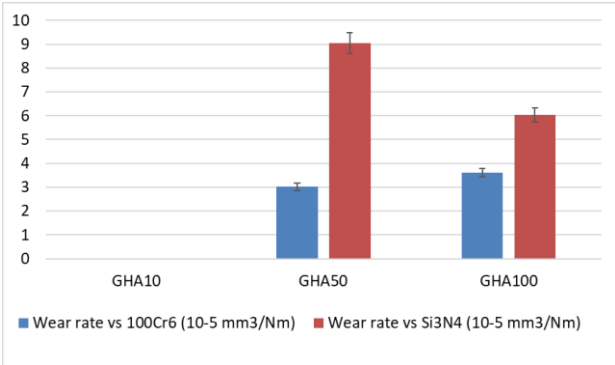

Figure 9. Values of the specific wear rate calculated for the samples, after sliding against 100Cr6 (blue columns) and Si_3N_4 (red columns) counterbodies.

From Figure 9 it is possible to highlight how the counterbody material had a strong influence on the wear rate of the considered samples. The high hardness of the silicon nitride balls results in a much higher degradation rate of the alumina porous layer, compared to the bearing steel ball, reaching an overall maximum of about 9 mm^3/Nm for the GHA50/Si_3N_4 tribocouple. It was not possible to calculate the wear rate of the thinnest sample (GHA10), because when sliding against bearing steel the counterbody adhered to the anodized surface, while during the test with the silicon nitride ball, the wear was negligible (Figure 8a).

3.3. Further Insights of the Wear Tracks

Backscattered electron (BSE) signal in the field emission gun scanning electron microscope (FEGSEM) was used, together with the energy dispersive spectroscopy, to clarify the adhesion of the chromium steel ball to the GHA10 sample (Figure 5a,d). Given the nature of the backscattered electrons, the contrast of the BSE micrographs is mainly given by the differences in the average atomic number of the elements. Therefore, as shown in Figure 10 the bright region corresponds to the chromium steel layer left on the ball trajectory by the counterbody, while the darker area is the GHA surface.

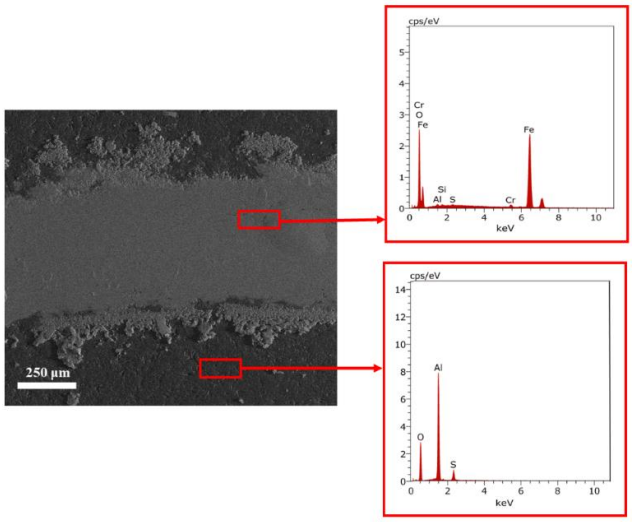

Figure 10. Backscattered electron (BSE) image of the GHA10/100Cr6 wear track with the microanalysis spectrum of the selected track area (**top**), and of the alumina coating (**bottom**).

This result was also confirmed by the energy dispersive spectroscopy (EDS) spectra reported in Figure 10; EDS spectrum taken inside the track showed peaks corresponding mainly to the Cr and Fe

characteristic energies, while the Al percentage was almost negligible. The EDS spectrum acquired outside the wear track highlighted the adhesion behavior of the counterbody material.

The backscattered electrons (BSE) signal was also used to investigate the surface of all the samples having flakes with similar features inside the wear tracks. As already known [48,49], when α-Al_2O_3 is exposed to high levels of humidity (75%, higher than the typical indoor values of 20–40%), the formation of aluminum hydroxide is likely to take place. In particular, the Al–O–OH form, already known as boehmite, has been found in previous works [50,51]. The BSE signal can be used to have evidence of the formation of this compound along with the flake generation.

Figure 11 shows the BSE micrographs of the GHA50/Si_3N_4 (Figure 11a) and GHA100/100Cr6 (Figure 11b) samples, which were taken as representative examples of the overall situation. The darker region could be identified as aluminum hydroxide, while the brightest part of the micrographs was alumina. These results are in agreement with those of the aluminum hydroxide formation theory, already reported in literature [50,51].

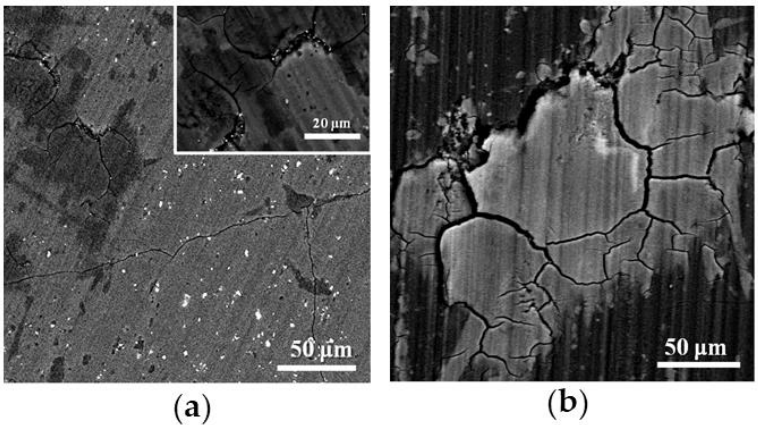

Figure 11. Backscattered electrons (BSE) micrograph of the worn surface of: (**a**) GHA50/Si_3N_4 (higher magnification of a detail in the inset), and (**b**) GHA100/100Cr6.

The wear tracks generated by the interaction with the Si_3N_4 counterbody (Figure 11a) showed the presence of a high amount of debris, whose brightness suggests that they were made of silicon nitride. This statement was also confirmed by EDS point analysis. In the inset of Figure 11a, the higher magnification of the details shows the presence of very fine wear debris inside the cracks generated by the sliding tests. Figure 11b shows, instead, the absence of debris throughout the wear track, while it is worth noting the presence of deep and randomly oriented cracks, only in the alumina regions (or rather the bright ones), leading to the generation of the flakes already detected by the secondary electrons signal (Figures 5 and 7).

The Fourier Transform Infrared Spectroscopy (FTIR) technique was used to confirm the aluminum hydroxide formation. Since spectra where overlapping, only the one corresponding to Figure 11b (GHA100/100Cr6) is reported in Figure 12, showing the occurrence of a strong broadening band due to hydrogen bonds with various hydroxyl groups (3770–3030 cm^{-1}), while the peak at 1081 cm^{-1} was linked to the Al–O vibrations.

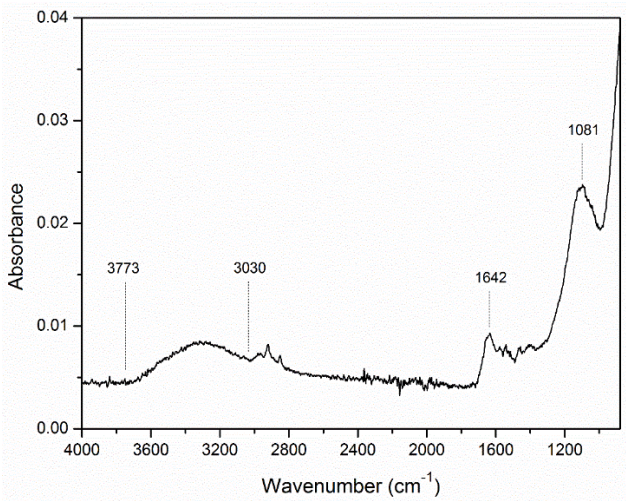

Figure 12. FTIR spectrum of the GHA100/100Cr6 samples wear track.

4. Discussion

Samples having anodized layer thickness of 10 µm (GHA10), 50 µm (GHA50) and 100 µm (GHA100) were prepared by hard anodization [44].

The surfaces were investigated by means of atomic force microscopy (AFM) and field emission gun scanning electron microscopy (FEGSEM), whose results, shown by Figures 1 and 2, demonstrated that by varying the thickness of the anodized samples, it is possible to modify the surface of the samples. Figure 1 highlights that while the GHA100 samples shows, at a micrometer level, surface features that can be described as a combination of those of the other two samples (GHA10 and GHA50), the GHA10 (Figure 1a) was the only one where circular elements were missing. As can be seen in Figure 2 the GHA10 sample also shows an irregular arrangement of the micrometric domains in which the pores were divided throughout the surface; furthermore, as highlighted in the inset of Figure 2a, in some areas of the sample's surface the porous structure seemed to collapse.

During hard anodization in order to increase the thickness, it is necessary to increase the time duration of the anodization process [43]. This did not affect remarkably the density and the dimensions of the pores [42], as suggested also by Figure 2 and its insets. In the considered samples what was changing remarkably was the arrangement of the micrometric domains, or rather the above-mentioned honeycomb-like structure typical of the GHA process [44]. The FEGSEM results of the surface inspections highlight that the duration of the anodization process to obtain a 10 µm thick alumina layer was too short to let the micrometric domains organize themselves (Figure 2a) in the most appropriate configuration, as those reached by the other samples (Figure 2b,c). These peculiarities seemed to have a strong impact on the sample's behavior, during the dry sliding under the chosen wear testing conditions.

As can be seen in Figure 4, indeed, the friction coefficient evolution shows a number of spikes, not spotted in the other measurements; the sliding resulted in the formation of the tribo-chemical layer observed in Figures 5a and 6a, causing a decrease of the friction coefficient to a steady-state sliding regime. The tribolayer formation was due to the counterbody adhesion on the alumina surface, and its composition was obtained by energy dispersive spectroscopy investigations, whose spectra are reported in Figure 10. The formation of tribo-chemical layers and their positive effect on the friction has been already reported by Kim et al. [14], during the study of nanoporous anodic aluminum oxide (AAO) reciprocating against steel balls (440C bearing steel) in dry sliding conditions, under high loads (0.1 N and 1 N). As can be seen in Figure 5a, the adhesion of the counterbody to the sample surface led to the steady-state wear regime, characterized only by small peaks related to the delamination of the tribo-chemical layer.

As observed by Malayoglu et al. [35] the formation of a tribolayer can be correlated with the asperities on the surface of the samples, providing the favorable conditions for the counterbody material adherence to the surface, owing to mechanical interlocking phenomena. The use of silicon nitride counterbodies under the same experimental conditions (Figure 5), highlighted the lack of tribo-chemical reactions at the ceramic/ceramic interface, despite the morphological features of the samples. Moreover, the hardness (1600 HV) of the silicon nitride counterbodies, considerably higher than that of the anodized samples (Table 2), results in a much higher degradation rate of the alumina porous layer (Figure 9), particularly remarkable for the sample having the lowest hardness overall (GHA50). The flakes generation inside the wear track was observed for all the samples (Figures 5 and 7), except for the GHA10/100Cr6 tribo-couple.

The formation of aluminum hydroxide, reported in Figure 11 and proved by the FTIR results in Figure 12, was found to be responsible for the flakes formation and showed to have a positive influence on the tribological properties of the samples, given its effect of limiting or rather avoiding the formation of cracks inside the wear tracks. The aluminum hydroxide formation during the α-Al_2O_3 dry sliding under high humidity conditions, firstly observed during the 90s [50,51] has been recently studied by Lee et al. [52] in tribotests performed under conditions like those used in the present study. The flake formation suggested that fracture and delamination of the coating seem to be the main wear mechanism.

Other studies reported in the literature from Yerokhin et al. [53] and Guezmil et al. [54] reported that anodic oxide coatings with low thicknesses are more effective in terms of friction, scratch and impact resistance. From the results highlighted in this paper, in terms of wear rate the GHA10 samples shows to have the best overall performance while sliding against the ceramic counterbody, since wear volume was so small to make the wear rate negligible. During the dry sliding test against the steel counterbody, the tribochemical reactions taking place at the interface between the anodized surface and the counterbody were the most influential parameter, since it caused adhesion in the case of the GHA10 sample (suggesting a link with the unique surface features of this sample). On the other hand, comparing the performance of the other two samples, the best overall behavior against 100Cr6 balls was ascribed to the thickest anodized sample (GHA100), probably due to the higher microhardness of the latter with respect to the 50 μm thick layer (GHA50).

The tribo-chemical reactions taking place during the dry sliding of the counterbodies on the anodized samples, due to the humidity and local temperature conditions, resulted in being enhanced by the morphological features of the anodized layers. This affects all the studied tribocouples and allows us to highlight the peculiar performance of the considered samples, which could expand their range of applicability.

5. Conclusions

The present paper investigated the wear resistance response of hard anodized aluminum, under unidirectional dry sliding conditions. Samples having alumina layer thicknesses of 10, 50 and 100 μm corresponding to the GHA10, GH50 and GHA100 names, obtained with the process reported in Reference [38], were subjected to wear tests in a pin-on-disk apparatus, using bearing steel (100Cr6) and ceramic (Si_3N_4) balls as counterbodies. The tribo-test results were correlated with the induced surface modifications. The main conclusions can be listed as follows:

When sliding against the bearing steel counterbody, the GHA10 sample shows the formation of a tribo-chemical layer, due to the adhesion of the counterbody material to the samples surface. On the other hand, the 50 μm (GHA50) thick sample showed a better performance compared to the thickest one (GHA100).

The dry sliding against the ceramic counterbodies resulted in a much higher degradation rate of the anodized layer with respect to the bearing steel balls, with the worst overall performance in terms of wear rate given by the GHA50 sample. This effect was ascribed to the lower hardness of this sample, while the thinnest anodized layer (GHA10) had the best performance with a negligible wear rate.

The results reported in the present paper show that the friction and wear behavior, as well as the wear mechanisms of the considered G.H.A. hard anodized AA6082 samples, were quite complex and varied strongly with the testing conditions. However, the superior performance of the sample with the thinnest anodized layer (GHA10), under the most demanding wear test (against Si_3N_4) requires further understanding since it could open interesting scenarios to foster the applicability of this peculiar anodization process.

Author Contributions: Conceptualization, A.M.S.H. and F.M.; methodology, M.C. and S.S.; validation, formal analysis, and investigation, E.S. and A.P.; writing—review and editing, E.S. All authors have read and agreed to the published version of the manuscript.

Funding: This research was made possible by a NPRP award NPRP 5–423–2–167 from the Qatar National Research Fund (a member of The Qatar Foundation).

Acknowledgments: The authors also acknowledge the support from Center for Advanced Materials (CAM) and Central Lab Unit (CLU) from Qatar University for the use of their facilities.

Conflicts of Interest: The authors declare no conflict of interest.

References

1. Hatch, J.E. *Aluminum: Properties and Physical Metallurgy*, 1st ed.; American Society for Metals: Cleveland, OH, USA, 1984.
2. Troeger, L.P.; Starke, E.A., Jr. Microstructural and mechanical characterization of a superplastic 6xxx aluminum alloy. *Mat. Sci. Eng. A* **2000**, *277*, 102–113. [CrossRef]
3. Marioara, C.D.; Andersen, S.J.; Jansen, J.; Zandbergen, H.W. The influence of temperature and storage time at RT on nucleation of the β″ phase in a 6082 Al–Mg–Si alloy. *Acta Mater.* **2003**, *51*, 789–796. [CrossRef]
4. Abdu, M.T.; Soliman, M.S.; El-Danaf, E.A.; Almajid, A.A.; Mohamed, F.A. Creep characteristics and microstructure in nano-particle strengthened AA6082. *Mat. Sci. Eng. A* **2012**, *531*, 35–44. [CrossRef]
5. Engler, O.; Hirsch, J. Texture control by thermomechanical processing of AA6xxx Al–Mg–Si sheet alloys for automotive applications—A review. *Mat. Sci. Eng. A* **2002**, *336*, 249–262. [CrossRef]
6. De Giorgi, M.; Scialpi, A.; Panella, F.W.; De Filippis, L.A.C. Effect of shoulder geometry on residual stress and fatigue properties of AA6082 FSW joints. *J. Mech. Sci. Technol.* **2009**, *23*, 26–35. [CrossRef]
7. Patil, H.S.; Soman, S.N. Experimental study on the effect of welding speed and tool pin profiles on AA6082-O aluminum friction stir welded butt joints. *Int. J. Eng. Sci. Technol.* **2010**, *2*, 268–275. [CrossRef]
8. Abdulstaar, M.; Mhaede, M.; Wagner, L. Pre-corrosion and surface treatments effects on the fatigue life of AA6082 T6. *Adv. Eng. Mater.* **2013**, *15*, 1002–1006. [CrossRef]
9. Hoar, T.P.; Mott, N.F. A mechanism for the formation of porous anodic oxide films on aluminum. *Phys. Chem. Solids.* **1959**, *9*, 97–99. [CrossRef]
10. Thompson, G.E. Porous anodic alumina: Fabrication, characterization and applications. *Thin Solid Films* **1997**, *297*, 192–201. [CrossRef]
11. Asoh, H.; Nishio, K.; Nakao, M.; Tamamura, T.; Masuda, H. Conditions for Fabrication of ideally ordered anodic porous alumina using pretextured Al. *J. Electrochem. Soc.* **2001**, *148*, B152–B156. [CrossRef]
12. Thompson, G.E.; Furneaux, R.C.; Wood, G.C.; Richardson, J.A.; Goode, J.S. Nucleation and growth of porous anodic films on aluminum. *Nature* **1978**, *272*, 433–435. [CrossRef]
13. Aerts, T.; Dimogerontakis, T.H.; De Graeve, I.; Fransaer, J.; Terryn, H. Influence of the anodizing temperature on the porosity and the mechanical properties of the porous anodic oxide film. *Surf. Coat. Technol.* **2007**, *201*, 7310–7317. [CrossRef]
14. Kim, H.S.; Kim, D.H.; Lee, W.; Cho, S.J.; Hahn, J.H.; Ahn, H.S. Tribological properties of nanoporous anodic aluminum oxide film. *Surf. Coat. Technol.* **2010**, *205*, 1431–1437. [CrossRef]
15. Hu, N.-N.; Ge, S.-H.; Fang, L. Tribological properties of nano-porous anodic aluminum oxide template. *J. Cent. South Univ. Technol.* **2011**, *18*, 1004–1008. [CrossRef]
16. Apachitei, L.E.F.; Duszczyk, J.; Katgerman, L. Vickers microhardness of AlSi(Cu) anodic oxide layers formed in H2SO4 at low temperature. *Surf. Coat. Techol.* **2003**, *165*, 309–315. [CrossRef]

17. Jia, Y.; Zhou, H.; Luo, P.; Luo, S.; Chen, J.; Kuang, Y. Preparation and characteristics of well-aligned macroporous films on aluminum by high voltage anodization in mixed acid. *Surf. Coat. Technol.* **2006**, *201*, 513–518. [CrossRef]
18. Sulka, G.D.; Parkola, K.G. Anodizing potential influence on well-ordered nanostructures formed by anodisation of aluminum in sulphuric acid. *Thin Solid Films* **2006**, *515*, 338–345. [CrossRef]
19. Moutarlier, V.; Gigandet, M.P.; Pagetti, J.; Normand, B. Influence of oxalic acid addition to chromic acid on the anodising of Al 2024 alloy. *Surf. Coat. Technol.* **2004**, *182*, 117–123. [CrossRef]
20. Bensalah, W.; Elleuch, K.; Feki, M.; De-Petris Wery, M.; Ayedi, H.F. Optimization of anodic layer properties on aluminum in mixed oxalic/sulphuric acid bath using statistical experimental methods. *Surf. Coat. Technol.* **2007**, *201*, 7855–7864. [CrossRef]
21. Bensalah, W.; Elleuch, K.; De-Petris Wery, M.; Ayedi, H.F. Comparative study of mechanical and tribological properties of alumina coatings formed on aluminum in various conditions. *Mater. Des.* **2009**, *30*, 3731–3737. [CrossRef]
22. Maejima, M.; Saruwataria, U.K.; Takaya, M. Friction behaviour of anodic oxide film on aluminum impregnated with molybdenum sulfide compounds. *Surf. Coat. Technol.* **2000**, *132*, 105–110. [CrossRef]
23. Takaya, M.; Hashimoto, K.; Toda, Y.; Maejima, M. Novel tribological properties of anodic oxide coating of aluminum impregnated with iodine compound. *Surf. Coat. Technol.* **2003**, *169*, 160–162. [CrossRef]
24. Riddar, F.; Kassman Rudolphi, Å. Comparison of friction performance of four anodized aluminum surfaces for use in a clutch actuator. *Wear* **2014**, *319*, 227–233. [CrossRef]
25. Wernick, S.; Pinner, R.; Sheasby, P.G. *The Surface Treatment and Finishing of Aluminium and its Alloys*, 6th ed.; Finishing Publications Ltd.: Teddington, UK, 1987.
26. Riddar, F.; Kassman Rudolphi, Å. Friction, wear and surface damage mechanisms of pneumatic clutch actuators. *Wear* **2013**, *305*, 36–44. [CrossRef]
27. Lee, G.-S.; Choi, J.H.; Choi, Y.C.; Bu, S.D.; Lee, Y.-Z. Tribological effects of pores on an anodized Al alloy surface as lubricant reservoir. *Curr. Appl. Phys.* **2011**, *11*, S182–S186. [CrossRef]
28. Liew, K.W.; Chia, S.Y.; Kok, C.K.; Low, K.O. Evaluation on tribological design coatings of Al2O3, Ni–P–PTFE and MoS2 on aluminum alloy 7075 under oil lubrication. *Mater. Des.* **2013**, *48*, 77–84. [CrossRef]
29. Tao, X.; Jianmin, C.; Jiazheng, Z.; Hongxi, D. The pore-enlargement and self-lubrication treatment of anodic oxide film of aluminum. *Wear* **1996**, *196*, 214–218. [CrossRef]
30. Skeldom, P.; Wang, H.W.; Thompson, G.E. Formation and characterization of self-lubricating MoS2 precursor films on anodized aluminum. *Wear* **1997**, *206*, 187–196. [CrossRef]
31. Tu, J.P.; Jiang, C.X.; Guo, S.Y.; Zhao, X.B.; Fu, M.F. Tribological properties of aligned film of amorphous carbon nanorods on AAO membrane in different environments. *Wear* **2005**, *259*, 759–764. [CrossRef]
32. Guezmil, M.; Bensalah, W.; Khalladi, A.; Elleuch, K.; De Petris-Wery, M.; Ayedi, H.F. Friction coefficient and microhardness of anodized aluminum alloys under different elaboration conditions. *Trans. Nonferrous Met. Soc. China* **2015**, *25*, 1950–1960. [CrossRef]
33. Picas, J.A.; Forn, A.; Ruperez, E.; Baile, M.T.; Martin, E. Hard Anodizing of aluminum matrix composite A6061/(Al2O3)p for wear and corrosion resistance improvement. *Plasma Processes Polym.* **2007**, *4*, S579–S583. [CrossRef]
34. Sieber, M.; Mehner, T.; Dietrich, D.; Alisch, G.; Nickel, D.; Meyer, D.; Scharf, I.; Lampke, T. Wear-resistant coatings on aluminum produced by plasma anodising—A correlation of wear properties, microstructure, phase composition and distribution. *Surf. Coat. Technol.* **2014**, *240*, 96–102. [CrossRef]
35. Malayoglu, U.; Tekin, K.C.; Malayoglu, U.; Shrestha, S. An investigation into the mechanical and tribological properties of plasma electrolytic oxidation and hard-anodized coatings on 6082 aluminum alloy. *Mat. Sci. Eng. A* **2011**, *528*, 7451–7460. [CrossRef]
36. Ovundur, M.; Muhaffel, F.; Cimenoglu, H. Characterization and tribological properties of hard anodized and micro arc oxidized 5754 quality aluminum alloy. *Tribol. Ind.* **2015**, *37*, 55–59.
37. Tsyntsaru, N.; Kavas, B.; Sort, J.; Urgen, M.; Celis, J.-P. Mechanical and frictional behaviour of nano-porous anodized aluminum. *Mater. Chem. Phys.* **2014**, *148*, 887–895. [CrossRef]
38. Vengatesh, P.; Kulandainathan, M.A. Hierarchically ordered self-lubricating superhydrophobic anodized aluminum surfaces with enhanced corrosion resistance. *ACS Appl. Mater. Interfaces* **2015**, *7*, 1516–1526. [CrossRef]

39. Dejun, K.; Jinchun, W.; Hao, L. Friction and wear performances of 7475 aluminium alloy after anodic oxidation. *Rare Met. Mater. Eng.* **2016**, *45*, 1122–1127. [CrossRef]
40. Lu, J.; Wei, G.; Yu, Y.; Guo, C.; Jiang, L. Aluminum alloy AA2024 anodized from the mixed acid system with enhanced mechanical properties. *Surf. Interface* **2018**, *13*, 46–50. [CrossRef]
41. Chen, L.; Li, Z.; Wang, B.; Song, Q.; Wan, Y.; Chen, L. Surface characterization and tribological performance of anodizing micro-textured aluminum-silicon alloys. *Materials* **2019**, *12*, 1862. [CrossRef]
42. Benea, L.; Dumitrascu, V. Enhancement in sustained friction and wear resistance of nanoporous aluminum oxide films obtained by controlled electrochemical oxidation process. *RSC Adv.* **2019**, *9*, 25056. [CrossRef]
43. Lee, W.; Ji, R.; Gösele, U.; Nielsch, K. Fast fabrication of long-range ordered porous alumina membranes by hard anodization. *Nat. Mater.* **2006**, *5*, 741–747. [CrossRef] [PubMed]
44. Ikeda, T.; Kinju, T.; Matsuo, Y. Method for surface treatment of aluminum or aluminum alloy. Japanese Patent N. EP1207220, 16 January 2008.
45. Bhushan, B. *Modern Tribology Handbook*, 1st ed.; CRC Press: Boca Raton, FL, USA, 2000.
46. ASTM G99-05(2010). *Standard Test Method for Wear Testing with a Pin-on-Disk Apparatus*; ASTM International: West Conshohocken, PA, USA, 2010.
47. Santecchia, E.; Cabibbo, M.; Hamouda, A.M.S.; Musharavati, F.; Popelka, A.; Spigarelli, S. Investigation of the temperature-related wear performance of hard nanostructured coatings deposited on a S600 high speed steel. *Metals* **2019**, *9*, 332. [CrossRef]
48. Perez-Unsueta, A.J.; Beynon, J.H.; Gee, M.G. The effect of surrounding atmosphere on the sliding wear of alumina. *Wear* **1991**, *146*, 179. [CrossRef]
49. Sasaki, S. The effects of the surrounding atmosphere on the friction and wear of alumina, zirconia, silicon carbide and silicon nitride. *Wear* **1989**, *134*, 185–200. [CrossRef]
50. Gee, M.G. The formation of aluminum hydroxide in the sliding wear of alumina. *Wear* **1992**, *153*, 201–227. [CrossRef]
51. Gee, M.G.; Jennett, N.M. High resolution characterisation of tribo-chemical films on alumina. *Wear* **1995**, *193*, 133–145. [CrossRef]
52. Lee, G.-S.; Cho, D.-H.; Kim, J.-S.; Kim, H.S.; Choi, Y.C.; Bu, S.D.; Lee, Y.-Z. Lubricating layer formed on porous anodic alumina template due to pore effect at water lubricated sliding and its properties. *Thin Solid Films* **2013**, *521*, 3–6. [CrossRef]
53. Yerokhin, A.L.; Nie, X.; Leyland, A.; Matthews, A.; Dowey, S.J. Plasma electrolysis for surface engineering. *Surf. Coat. Technol.* **1999**, *122*, 73–93. [CrossRef]
54. Guezmil, M.; Bensalah, W.; Khalladi, A.; Elleuch, K.; De-Petris Wery, M.; Ayedi, H.F. Effect of test parameters on the friction behaviour of anodized aluminium alloy. *Int. Schol. Res. Notices* **2014**, *2014*, 795745. [CrossRef]